Control of Physical Parameters in Binary Black Hole Initial Data

Iago Mendes[1,2]

Mentors: Nils Vu[1], Mark Scheel[1], Saul Teukolsky[1,3]

[1]Theoretical Astrophysics 350-17, California Institute of Technology, Pasadena, CA 91125, USA
[2]Department of Physics and Astronomy, Oberlin College, Oberlin, Ohio 44074, USA
[3]Cornell Center for Astrophysics and Planetary Science, Cornell University, Ithaca, New York 14853, USA

This report was submitted as part of the Summer Undergraduate Research Fellowship (SURF) program at Caltech.

(Dated: September 24, 2024)

Abstract

When solving Einstein's equations for Binary Black Holes (BBH) numerically, we split the four-dimensional spacetime into three-dimensional spatial slices and evolve them over time. The first slice is described by solving an Initial Data problem, which is cast as five elliptic partial differential equations in the extended conformal thin-sandwich (XCTS) decomposition. Prior to solving the XCTS equations, we must choose "free data" to impose boundary conditions and specify background quantities. This is the approach taken in `SpECTRE`, a parallel code that aims to simulate BBH for the new generations of gravitational wave detectors. After solving the XCTS system, `SpECTRE` runs a horizon finder that measures the masses and spins of the black holes. Additionally, our work extends `SpECTRE`'s capabilities to calculate total energy, momentum, and center of mass as infinite integrals using the Arnowitt-Deser-Misner (ADM) formalism. Typically, we want to choose these physical quantities before running a BBH simulation, but they can only be measured after numerically solving the XCTS equations. To address this, we implemented an iterative scheme in `SpECTRE` that drives the physical parameters to their desired values by adjusting the free data in a quasi-Newton-Raphson method that efficiently computes the Jacobian with Broyden's method.

1. Introduction

In the early twentieth century, Einstein revolutionized the study of gravity by connecting spacetime geometry with physical dynamics. As John Wheeler says, "Spacetime tells matter how to move; matter tells spacetime how to curve" [1]. Being a highly complex theory, many problems of interest only have analytic solutions in special cases with symmetry. In this context, Numerical Relativity emerged as an essential field to solve these problems numerically, allowing us to explore general cases that can be found in

the universe. Specifically, simulations of Binary Black Holes (BBH) became very important as gravitational wave detectors were developed, needing to use numerical results to identify and characterize signals in their data [2].

Famously, the Einstein equations relate the curvature of spacetime to the stress-energy of matter, forming a system of ten nonlinear partial differential equations (PDEs). With the 3+1 formalism, we can rearrange these equations so that spacetime is described by spacelike three-dimensional slices of constant time [3]. In doing so, we find that four out of the ten equations do not involve time derivatives, implying that they are constraints that must be satisfied at all times. The remaining six equations describe an evolution of the constraint-satisfying fields. Using this formalism, the Spectral Einstein Code (`SpEC`) [4] runs BBH simulations by first finding initial data and then running an evolution on them. Over time, as `SpEC` faced more challenging BBH with high mass ratios and spins, several improvements had to be made to the initial data techniques, which are summarized in [5].

Despite its success in BBH simulations, `SpEC` shows its limitations in more challenging problems, such as binary neutron star mergers and BBH with extreme configurations. In this context, `SpECTRE` [6] was created as a codebase that follows a better parallelism model and aims to be more scalable [7]. Previous work has already shown that `SpECTRE` can be faster and more accurate than `SpEC` when performing similar tasks due to its use of parallelism [8]. This will be especially needed for the upcoming gravitational wave detectors with higher sensitivity, such as the Cosmic Explorer, the Einstein Telescope and LISA.

As part of an effort to allow researchers to fully simulate BBH in `SpECTRE`, an initial data procedure similar to the one in `SpEC` needs to be completed. This is greatly benefitted by a scalable elliptic solver that was recently developed [8], which can now be used to solve the initial data equations. Be that as it may, before the start of the SURF program, `SpECTRE` did not have a way to enforce specific masses and spins for the black holes or to avoid drifts in their orbital trajectories. This report describes how we addressed these issues.

[TO-DO: Explain the purpose of each section]

2. Background

[TO-DO: Introduce 3+1 decomposition and the ADM formalism, referring to Figure 1]

[TO-DO: Talk about conformal decomposition and the XCTS equations]

[TO-DO: Mention SKS and free data, referring to Figure 2]

3. Methods

3.1. Calculation of asymptotic quantities

In Newtonian mechanics, it is typically straightforward to compute the center of mass and the linear momentum of a system. However, in general relativity, these are

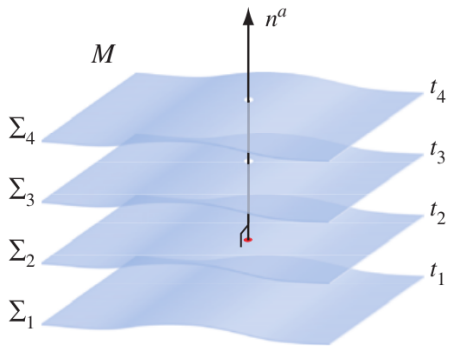

Figure 1: Foliation of 4D spacetime into 3D spatial slices at different times. This image is originally from Figure 2.1 in [9].

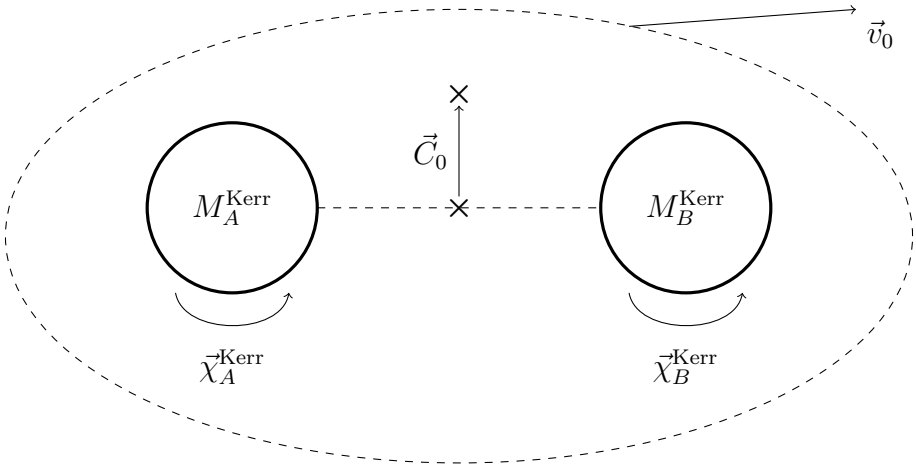

Figure 2

asymptotic quantities – defined by infinite surface integrals. Since the computational domains are coarser at their outer boundaries, these integrals tend to be very sensitivity to small errors, leading to less accurate results. To overcome this, we can cast these calculations as volume integrals using Gauss' theorem. Below, we explain the approaches we used to compute these asymptotic quantities in `SpECTRE`.

We can measure the total energy of a system by computing the ADM mass $M_{\rm ADM}$. In terms of conformal quantities, it takes the form of

$$M_{\rm ADM} = \frac{1}{16\pi} \oint_{S_\infty} \left(\bar{\gamma}^{jk} \bar{\Gamma}^i_{jk} - \bar{\gamma}^{ij} \bar{\Gamma}_j - 8 \bar{D}^i \psi \right) d\bar{S}_i \tag{1}$$

[9, Eq. 3.139], where $\bar{\Gamma}^i_{jk}$ are the Christoffel symbols associated with $\bar{\gamma}_{ij}$ (see Eq. 2.44 in

[9] for a definition) and $\bar{\Gamma}_j = \bar{\Gamma}^i_{ij}$. Applying Gauss' theorem to Eq. (1), we have

$$M_{\rm ADM} = \frac{1}{16\pi}\int_{V_\infty} \bar{D}_i\Big(\bar{\gamma}^{jk}\bar{\Gamma}^i_{jk} - \bar{\gamma}^{ij}\bar{\Gamma}_j - 8\bar{D}^i\psi\Big)\, d\bar{V} \tag{2}$$

$$= \frac{1}{16\pi}\int_{V_\infty} \Big(\partial_i\bar{\gamma}^{jk}\bar{\Gamma}^i_{jk} + \bar{\gamma}^{jk}\partial_i\bar{\Gamma}^i_{jk} + \bar{\Gamma}_l\bar{\gamma}^{jk}\bar{\Gamma}^l_{jk} - \partial_i\bar{\gamma}^{ij}\bar{\Gamma}_j - \bar{\gamma}^{ij}\partial_i\bar{\Gamma}_j - \bar{\Gamma}_l\bar{\gamma}^{lj}\bar{\Gamma}_j - 8\bar{D}^2\psi\Big) d\bar{V}, \tag{3}$$

where we can use the Hamiltonian constraint to replace $8\bar{D}^2\psi$ with

$$8\bar{D}^2\psi = \psi\bar{R} + \frac{2}{3}\psi^5 K^2 - \frac{1}{4}\psi^5\frac{1}{\alpha^2}\Big[(\bar{L}\beta)_{ij} - \bar{u}_{ij}\Big]\Big[(\bar{L}\beta)^{ij} - \bar{u}^{ij}\Big] - 16\pi\psi^5\rho \tag{4}$$

[9, Eq. 3.37].

Using the formalism developed in [10], we can find the center of mass of a system by evaluating the integral

$$C^i_{\rm CoM} = \frac{3}{8\pi M_{\rm ADM}}\oint_{S_\infty} \psi^4 n^i\, dA \tag{5}$$

[5, Eq. 26], where $n^i = x^i/r$ and $r = \sqrt{x^2+y^2+z^2}$. Applying Gauss' theorem to Eq. (5), we have

$$C^i_{\rm CoM} = \frac{3}{8\pi M_{\rm ADM}}\oint_{S_\infty} \partial_j\Big(\psi^4 n^i n^j\Big)\, dV \tag{6}$$

$$= \frac{3}{4\pi M_{\rm ADM}}\int_{V_\infty} \frac{1}{r^2}\Big(2\psi^3\partial_j\psi x^i x^j + \psi^4 x^i\Big) dV. \tag{7}$$

We can also measure the total linear momentum of a system with the ADM linear momentum $P^i_{\rm ADM}$ using the expressions derived in [5, Eqs. 18–22]. As an infinite surface integral, it is expressed as

$$P^i_{\rm ADM} = \frac{1}{8\pi}\oint_{S_\infty} \psi^{10}\Big(K^{ij} - K\gamma^{ij}\Big)\, dS_j. \tag{8}$$

Applying Gauss' theorem and using the momentum constraint, it becomes

$$P^i_{\rm ADM} = \frac{1}{8\pi}\oint_{S_\infty} \partial_j\Big[\psi^{10}\Big(K^{ij} - K\gamma^{ij}\Big)\Big]\, dV \tag{9}$$

$$= -\frac{1}{8\pi}\int_{V_\infty} \Big[\bar{\Gamma}^i_{jk}P^{jk} + \bar{\Gamma}^j_{jk}P^{jk} - 2\bar{\gamma}_{jk}P^{jk}\bar{\gamma}^{il}\partial_l(\ln\psi)\Big]\, dV, \tag{10}$$

where $P^{ij} = \psi^{10}(K^{ij} - K\gamma^{ij})$ is the integrand of Eq. (8). Note that the matter sources are ignored when using the momentum constraint in [9], but it is straightforward to add the source term to Eq. (10) is needed in the future.

An attentive reader might have noticed that we have used Gauss' theorem in two different ways. That is, we used the conformal covariant derivative $\bar{D}_i$ and the conformal volume element $d\bar{V}$ in Eq. (2), but the partial derivative ∂_i and the Euclidean volume

element dV in Eq. (6) and Eq. (9). Both approaches are equivalent [11, 12], as long as we are consistent.

In practice, we cannot `SpECTRE` cannot evaluate volume integrals over all space because the interior of the black holes are excised from the domain. Hence, if we wish to use the infinite volume integrals, we must still perform finite surface integrals enclosing the excisions. For practicality, we choose to do such integrals over the excisions themselves. If we let S_0 be the combination of the excision surfaces, the resulting computations become

$$\begin{aligned} M_{\mathrm{ADM}} = &\frac{1}{16\pi}\oint_{S_0}\left(\bar{\gamma}^{jk}\bar{\Gamma}^i_{jk} - \bar{\gamma}^{ij}\bar{\Gamma}_j - 8\bar{D}^i\psi\right)d\bar{S}_i \\ &+ \frac{1}{16\pi}\int_{V_\infty}\Big(\partial_i\bar{\gamma}^{jk}\bar{\Gamma}^i_{jk} + \bar{\gamma}^{jk}\partial_i\bar{\Gamma}^i_{jk} + \bar{\Gamma}_l\bar{\gamma}^{jk}\bar{\Gamma}^l_{jk} \\ &\qquad - \partial_i\bar{\gamma}^{ij}\bar{\Gamma}_j - \bar{\gamma}^{ij}\partial_i\bar{\Gamma}_j - \bar{\Gamma}_l\bar{\gamma}^{lj}\bar{\Gamma}_j - 8\bar{D}^2\psi\Big)d\bar{V}, \end{aligned} \tag{11}$$

$$\begin{aligned} C^i_{\mathrm{CoM}} = &\frac{3}{8\pi M_{\mathrm{ADM}}}\oint_{S_0}\psi^4 n^i\, dA \\ &+ \frac{3}{4\pi M_{\mathrm{ADM}}}\int_{V_\infty}\frac{1}{r^2}\Big(2\psi^3\partial_j\psi x^i x^j + \psi^4 x^i\Big)dV, \end{aligned} \tag{12}$$

$$\begin{aligned} P^i_{\mathrm{ADM}} = &\frac{1}{8\pi}\oint_{S_0}\psi^{10}\Big(K^{ij} - K\gamma^{ij}\Big)\,dS_j \\ &- \frac{1}{8\pi}\int_{V_\infty}\Big[\bar{\Gamma}^i_{jk}P^{jk} + \bar{\Gamma}^j_{jk}P^{jk} - 2\bar{\gamma}_{jk}P^{jk}\bar{\gamma}^{il}\partial_l(\ln\psi)\Big]\,dV. \end{aligned} \tag{13}$$

Because of `SpECTRE`'s task-based parallelism, we must first evaluate the integrals locally in each domain element. Then, we perform a reduction to combine the results from all elements into a single result for the entire domain.

3.2. Control loop

Once the XCTS equations are solved, we have all the information that we need about the zero-time slice of spacetime. With this, we can use an apparent horizon finder to get measurements of the black holes in the constructed initial data. Let M_A, M_B, $\vec{\chi}_A$ and $\vec{\chi}_B$ be the masses and spins of the actual black holes that we have been able to create. In general, these values will differ from the "target" quantities M^*_A, M^*_B, $\vec{\chi}^*_A$ and $\vec{\chi}^*_B$. For example, suppose that we wish to simulate an equal-mass non-spinning case with $M^*_A = M^*_B = 0.5$ and $\vec{\chi}^*_A = \vec{\chi}^*_B = (0,0,0)$. In order to construct the SKS analytical expressions, it is natural to specify $M^{\mathrm{Kerr}}_{A,B} = M^*_{A,B}$ and $\vec{\chi}^{\mathrm{Kerr}}_{A,B} = \vec{\chi}^*_{A,B}$. With this, we can solve the XCTS equations and find horizons in the resulting initial data. Once we do it in `SpECTRE`, we find that the resulting black hole parameters are actually $M_{A,B} \approx 0.6$ and $\vec{\chi}_{A,B} \approx (0,0,-0.002)$.

If we measure the asymptotic quantities described in the previous subsection, we might find that they are also not desirable. Ideally, $\vec{C}_{\mathrm{CoM}}$ and $\vec{P}_{\mathrm{ADM}}$ should be equal to zero in order to minimize any drifts of the binary orbit, especially for long simulations. However, similar to the example above, we can only know these quantities after the initial data has been constructed.

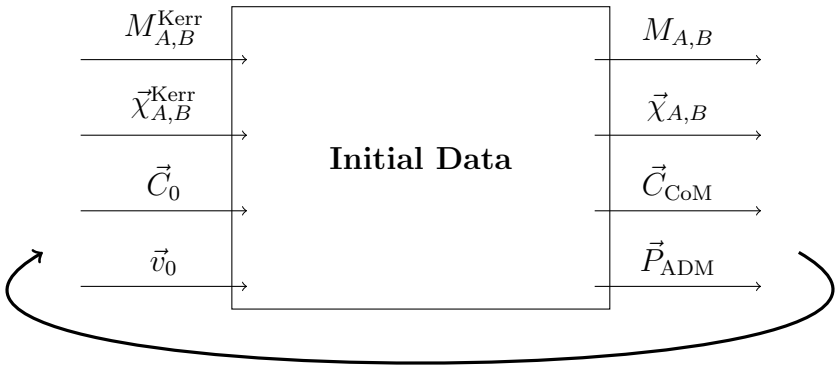

Figure 3: Schematic representation of the control loop.

Note that $M_{A,B}$, $\vec{\chi}_{A,B}$, $\vec{C}_{\rm CoM}$ and $\vec{P}_{\rm ADM}$ are the parameters that we wish to control, but we cannot directly set them to the desired values. We handle this issue is by iterating over different choices of the free data ($M^{\rm Kerr}_{A,B}$, $\vec{\chi}^{\rm Kerr}_{A,B}$, $\vec{C}_0$ and $\vec{v}_0$), trying to find the ones that result in the ideal physical parameters. Figure 3 shows a schematic representation of this "control loop".

Let the choices of the free data be represented as

$$\begin{aligned}\mathbf{u} = \Big(&M_A^{\rm Kerr}, M_B^{\rm Kerr}, \chi_A^{{\rm Kerr},x}, \chi_A^{{\rm Kerr},y}, \chi_A^{{\rm Kerr},z},\\ &\chi_B^{{\rm Kerr},x}, \chi_B^{{\rm Kerr},y}, \chi_B^{{\rm Kerr},z}, C_0^x, C_0^y, C_0^z, v_0^x, v_0^y, v_0^z\Big).\end{aligned} \tag{14}$$

Also, let the difference between the current and target physical parameters be represented as

$$\begin{aligned}\mathbf{F}(\mathbf{u}) = \Big(&M_A - M_A^*, M_B - M_B^*, \chi_A^x - \chi_A^{*,x}, \chi_A^y - \chi_A^{*,y}, \chi_A^z - \chi_A^{*,z},\\ &\chi_B^x - \chi_B^{*,x}, \chi_B^y - \chi_B^{*,y}, \chi_B^z - \chi_B^{*,z}, C^x_{\rm CoM}, C^y_{\rm CoM}, C^z_{\rm CoM}, P^x_{\rm ADM}, P^y_{\rm ADM}, P^z_{\rm ADM}\Big).\end{aligned} \tag{15}$$

As discussed in the example above, it is natural to use the target values as an initial guess for the free data:

$$\begin{aligned}\mathbf{u}_0 = \Big(&M_A^*, M_B^*, \chi_A^{*,x}, \chi_A^{*,y}, \chi_A^{*,z},\\ &\chi_B^{*,x}, \chi_B^{*,y}, \chi_B^{*,z}, 0, 0, 0, 0, 0, 0\Big).\end{aligned} \tag{16}$$

With this, we can update our free data at every control iteration $k \geq 1$ using a Newton-Raphson scheme [13]:

$$\mathbf{u}_k = \mathbf{u}_{k-1} - \mathbb{J}^{-1}_{k-1} \cdot \mathbf{F}_{k-1}. \tag{17}$$

Note however that each evaluation of $\mathbf{F}(\mathbf{u})$ is computationally expensive as it requires an entire Initial Data solve. Therefore, computing the Jacobian in Eq. (17) analytically

is unfeasible. That said, we can find it numerically using Broyden's method [13]:

$$\mathbb{J}_k = \mathbb{J}_{k-1} + \frac{\mathbf{F}_k \otimes \Delta\mathbf{u}_k}{||\Delta\mathbf{u}_k||^2}, \tag{18}$$

where $\Delta\mathbf{u}_k = \mathbf{u}_k - \mathbf{u}_{k-1}$.

Since we're iteratively computing the Jacobian with Eq. (18), we must choose an adequate initial guess $\mathbb{J}_0$. Assume that $M_{A,B}|_0 \approx M^{\rm Kerr}_{A,B}|_0$ and $\vec{\chi}_{A,B}|_0 \approx \vec{\chi}^{\rm Kerr}_{A,B}|_0$, then

$$\left.\frac{\partial(M_{A,B} - M^*_{A,B})}{\partial M^{\rm Kerr}_{A,B}}\right|_0 \approx \left.\frac{\partial(\chi^i_{A,B} - \chi^{*,i}_{A,B})}{\partial \chi^{{\rm Kerr},i}_{A,B}}\right|_0 \approx 1. \tag{19}$$

Using a Newtonian center of mass approximation, we know that

$$\vec{C}_{\rm CoM} \approx \frac{M_A\vec{c}_A + M_B\vec{c}_B}{M_A + M_B} + \vec{C}_0, \tag{20}$$

where $\vec{c}_{A,B}$ are the centers of black holes A and B. Note that we choose $\vec{c}_{A,B}$ so that

$$\frac{M_A\vec{c}_A + M_B\vec{c}_B}{M_A + M_B} = 0. \tag{21}$$

Hence,

$$\left.\frac{\partial(C^i_{\rm CoM})}{\partial C^i_0}\right|_0 \approx 1. \tag{22}$$

We can also use a Newtonian linear momentum approximation:

$$\vec{P}_{\rm ADM} \approx (M_A + M_B)\Big[(\vec{\Omega}_0 \times \vec{C}_{\rm CoM}) + \dot{a}_0\vec{C}_{\rm CoM} + \vec{v}_0\Big], \tag{23}$$

where $\vec{\Omega}_0$ is the initial angular velocity and $\vec{\dot{a}}_0$ is the initial radial expansion velocity[1]. Typically, these initial orbit parameters are small and $M_A + M_B \approx 1$ in code units. Then,

$$\left.\frac{\partial(P^i_{\rm ADM})}{\partial v^i_0}\right|_0 \approx 1. \tag{24}$$

All the other partial derivatives that go into $\mathbb{J}_0$ are approximately zero under the assumptions imposed above. Therefore, a good initial guess for the Jacobian is

$$\mathbb{J}_0 \approx \mathbb{I}, \tag{25}$$

a 14-by-14 identity matrix.

[1]These initial orbit parameters show up here because they are added to the boundary condition of the shift β^i.

4. Results

4.1. Convergence of asymptotic quantities

We have tested our calculation of asymptotic quantities with analytic solutions of a single black hole, as well as with a numeric solution to the XCTS equations for BBH. We use analytic solutions that describe a Schwarzschild black hole of mass M in:

- Isotropic coordinates;
- Isotropic coordinates with a boost speed v;
- Kerr-Schild coordinates;
- Kerr-Schild coordinates with a boost speed v.

For the unboosted analytic solutions, the expected values of M_{ADM} and P_{ADM} are

$$M_{\mathrm{ref}} = M \tag{26}$$

and

$$P_{\mathrm{ref}} = 0. \tag{27}$$

For the boosted analytic solutions, the expected values of M_{ADM} and P_{ADM} are

$$M_{\mathrm{ref}} = \gamma M \tag{28}$$

and

$$P_{\mathrm{ref}} = \gamma M v, \tag{29}$$

where $\gamma = 1/\sqrt{1-v^2}$ is the Lorentz factor. We also use a BBH solution for an equal-mass non-spinning case, implying that the expected value of P_{ADM} is

$$P_{\mathrm{ref}} = 0. \tag{30}$$

Since we do not know the expected value of M_{ADM} for the BBH solution, we use the result at the largest outer radius R as a reference:

$$M_{\mathrm{ref}} = M_{\mathrm{ADM}}|_{\max R}. \tag{31}$$

Figure 4 compares the difference between the measured M_{ADM} and P_{ADM} with the reference values M_{ref} and P_{ref}, as described in the previous paragraph. For each subplot, we see how this residual evolves as we increase the outer radius R of the domain, which serves as "infinity" in these calculations. Since these quantities are defined asymptotically, we should approach the reference values as R increases. Excluding trivial cases (in which the residuals already start very low), we see that the infinite surface integrals defined in Eq. (1) and Eq. (8) convergence just as expected. However, this is not the case for the finite surface integrals and infinite volume integrals defined in Eq. (11) and Eq. (13). Specifically, we see that the results do not convergence at all for the boosted cases. Other than that, this approach behaves as expected.

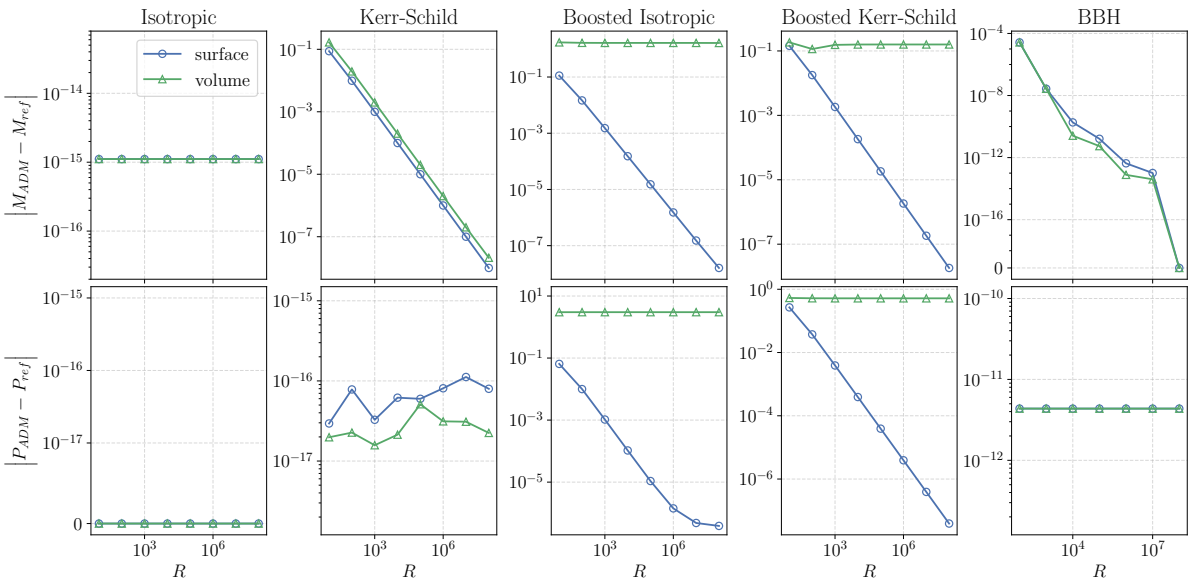

Figure 4: Convergence with distance for M_{ADM} and P_{ADM}. "Surface" indicates results from evaluating the infinite surface integrals defined in Eq. (1) and Eq. (8). "Volume" indicates results from evaluating the finite surface integrals and the infinite volume integrals defined in Eq. (11) and Eq. (13).

To study the center of mass calculations, we need a different analysis. First, the Kerr-Schild solutions do not fall off to flatness fast enough to satisfy the assumptions for Eq. (5) to hold. Second, the expected $\vec{C}_{\mathrm{CoM}}$ value for the Isotropic and BBH solutions are zero, so we need to shift the solution to get a non-vanishing result. Figure 5 shows some useful results taking these points into consideration.

An important feature in Figure 5 is that the results seem to diverge from the expected value as we increase R. We do not fully understand why this occurs, but our hypothesis is that there is a round-off error in the nature of this calculation that grows substantially as we increase R. One way to interpret Eq. (5) is that we are summing over the unit vectors n^i, rescaled by ψ^4, in all directions. If $\psi(\vec{r})$ is constant, no rescaling happens and all the unit vectors cancel out. If $\psi(\vec{r})$ is not constant, then $\vec{C}_{\mathrm{CoM}}$ will emerge from the difference of large numbers. With larger and larger numbers being involved in this cancellation (i.e. with increasing R), we loose numerical accuracy. In other words, we are seeking the subdominant terms. This hypothesis makes sense when we look at the residuals of the shifted solutions. We see that the results converge as we increase R until when the residuals reach the level of round-off errors (indicated by the residuals of the unshifted solutions).

Comparing the "volume" residuals with the "surface" residuals, we see that Eq. (12) leads to higher round-off errors than Eq. (5). This also makes sense because the volume integral involves many more elements. However, we notice a strange behavior of the C^x_{CoM} "volume" residuals for the unshifted BBH solution. For that specific case, we see that the x component of Eq. (12) diverges since the beginning, which does not occur

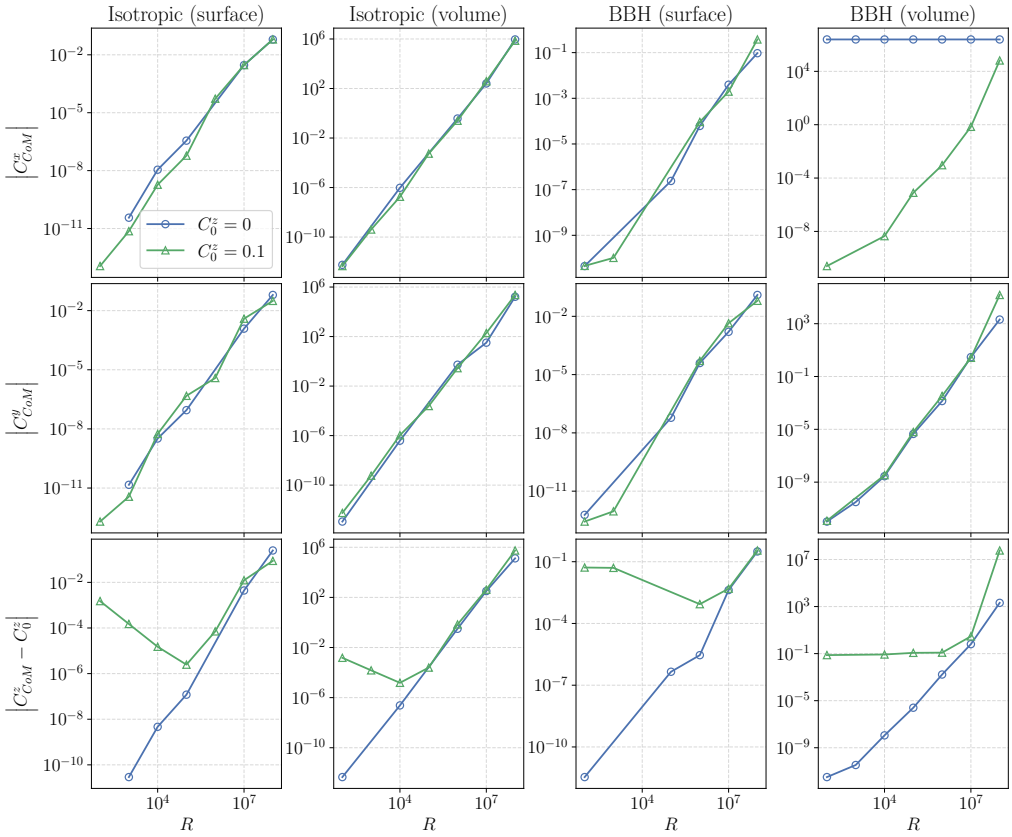

Figure 5: Convergence with distance for $\vec{C}_{\mathrm{CoM}}$. "Surface" indicates results from evaluating the infinite surface integral defined in Eq. (5). "Volume" indicates results from evaluating the finite surface integral and the infinite volume integral defined in Eq. (12). Residuals for each component of $\vec{C}_{\mathrm{CoM}}$ are shown for an unshifted solution ($C^z_0 = 0$) and for a shifted solution ($C^z_0 = 0.1$).

anymore if a z-shift is added to the solution. This might be an indication of a bug in the implementation of the method.

Apart from knowing that we approach the expected values for increasing R, we must confirm that the results get more accurate with resolution. Figure 6 shows that the residuals in general converge exponentially with polynomial order P and converge faster with higher refinement level L, as expected for the Discontinuous Galerkin scheme used in `SpECTRE` [14]. Some C_{CoM} convergence plots do not follow this trend, but this seems to occur when the residual levels are close to the round-off errors seen in Figure 5.

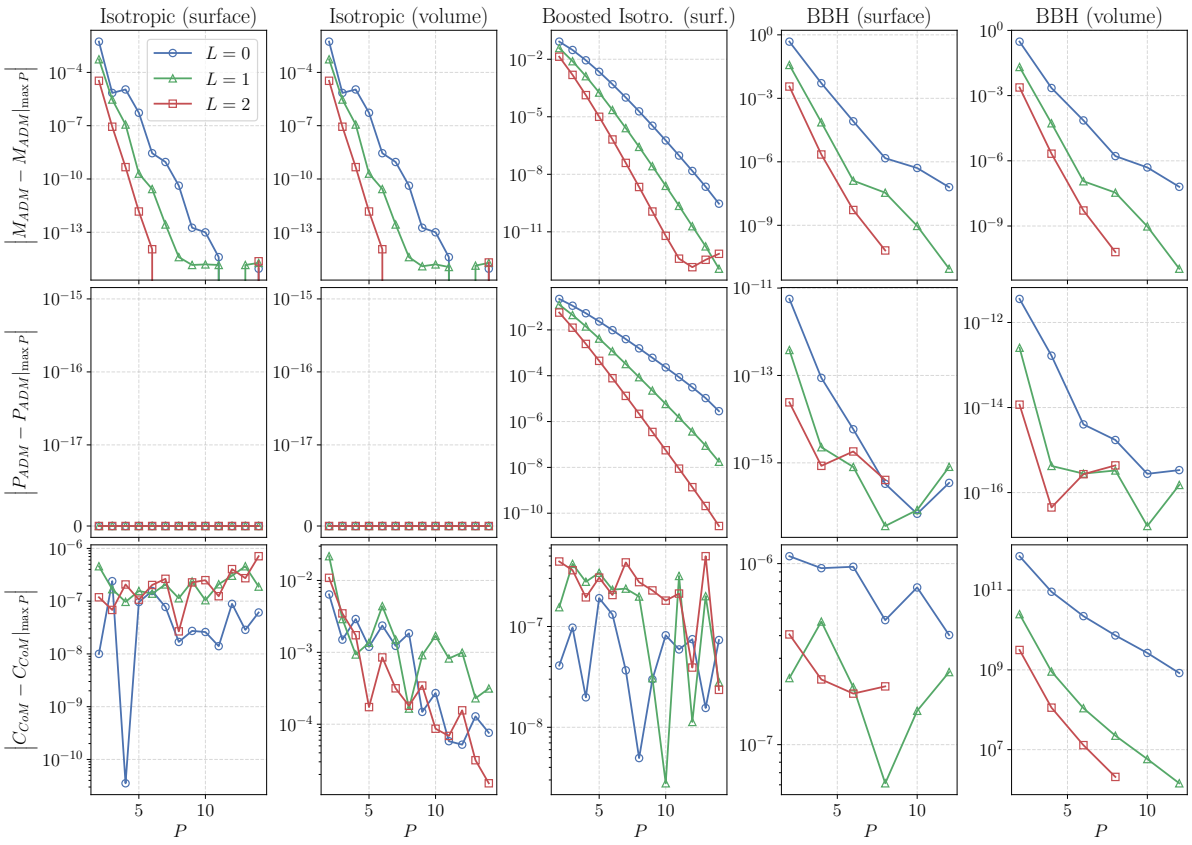

Figure 6: Convergence with resolution for M_{ADM}, P_{ADM}, and C_{CoM}. Each subplot shows the difference at each polynomial order P relative to the highest P result for multiple refinement levels L.

4.2. Control iterations

5. Conclusion

Acknowledgements

References

[1] John Wheeler and Kenneth Ford. "Geons, Black Holes and Quantum Foam: A Life in Physics". In: *American Journal of Physics* 68 (June 2000). DOI: 10.1119/1.19497.

[2] B. P. Abbott et al. "Observation of Gravitational Waves from a Binary Black Hole Merger". In: *Phys. Rev. Lett.* 116 (6 Feb. 2016), p. 061102. DOI: 10.1103/PhysRevLett.116.061102.

[3] Miguel Alcubierre. *Introduction to 3+1 Numerical Relativity*. Oxford University Press, Apr. 2008. ISBN: 9780199205677. DOI: 10.1093/acprof:oso/9780199205677.001.0001.

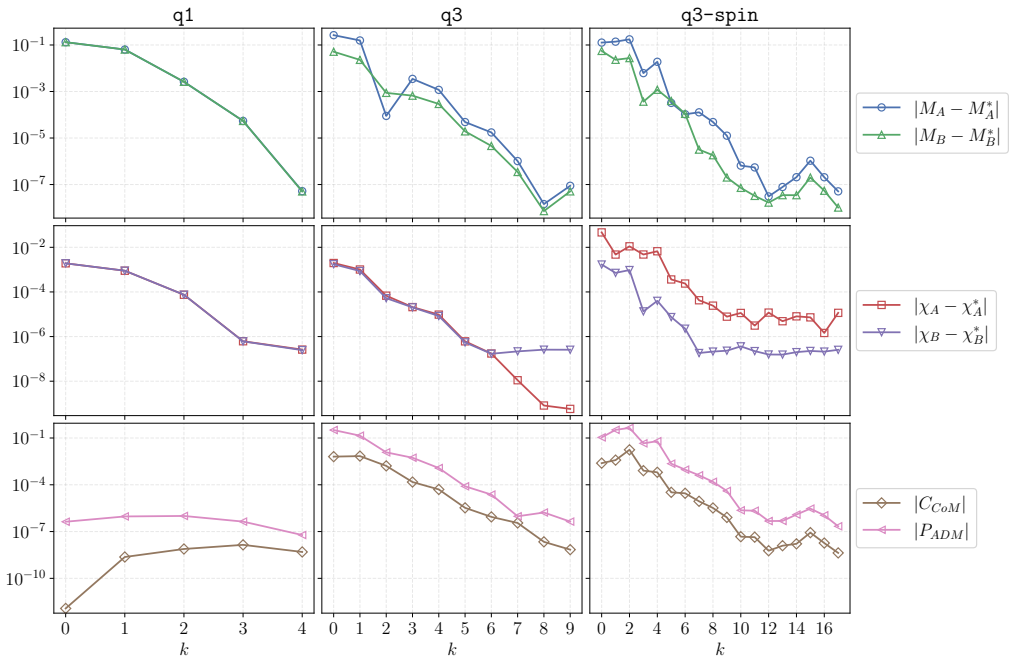

Figure 7

[4] Lawrence Kidder, Harald Pfeiffer, Mark Scheel, et al. *Spectral Einstein Code (SpEC)*. URL: https://black-holes.org/code/SpEC.

[5] Serguei Ossokine, Francois Foucart, Harald P Pfeiffer, et al. "Improvements to the construction of binary black hole initial data". In: *Classical and Quantum Gravity* 32.24 (Dec. 2015), p. 245010. ISSN: 1361-6382. DOI: 10.1088/0264-9381/32/24/245010.

[6] Nils Deppe, William Throwe, Lawrence E. Kidder, et al. *SpECTRE*. Version 2024.02.05. Feb. 2024. DOI: 10.5281/zenodo.10619885. URL: https://spectre-code.org.

[7] Lawrence E. Kidder, Scott E. Field, Francois Foucart, et al. "SpECTRE: A task-based discontinuous Galerkin code for relativistic astrophysics". In: *Journal of Computational Physics* 335 (2017), pp. 84–114. ISSN: 0021-9991. DOI: 10.1016/j.jcp.2016.12.059.

[8] Nils L. Vu, Harald P. Pfeiffer, Gabriel S. Bonilla, et al. "A scalable elliptic solver with task-based parallelism for the SpECTRE numerical relativity code". In: *Phys. Rev. D* 105 (8 Apr. 2022), p. 084027. DOI: 10.1103/PhysRevD.105.084027.

[9] Thomas W. Baumgarte and Stuart L. Shapiro. *Numerical Relativity: Solving Einstein's Equations on the Computer*. Cambridge University Press, 2010. ISBN: 9781139193344. DOI: 10.1017/CBO9781139193344.

[10] D. Baskaran, S.R. Lau, and A.N. Petrov. "Center of mass integral in canonical general relativity". In: *Annals of Physics* 307.1 (2003), pp. 90–131. ISSN: 0003-4916. DOI: 10.1016/S0003-4916(03)00062-9.

[11] Andrew DeBenedictis. "Integration in General Relativity". In: (1998). arXiv: physics/9802027 [math-ph].

[12] Saul A. Teukolsky. "Formulation of discontinuous Galerkin methods for relativistic astrophysics". In: *Journal of Computational Physics* 312 (2016), pp. 333–356. ISSN: 0021-9991. DOI: 10.1016/j.jcp.2016.02.031.

[13] William H. Press et al. *Numerical Recipes 3rd Edition: The Art of Scientific Computing*. Cambridge University Press, 2007. ISBN: 0521880688. URL: https://numerical.recipes.

[14] Jan Hesthaven and Tim Warburton. "Nodal Discontinuous Galerkin Methods: Algorithms, Analysis, and Applications". In: vol. 54. Jan. 2007. DOI: 10.1007/978-0-387-72067-8.